Chinese Journal of Chemical Engineering 56 (2023) 119–125

Contents lists available at ScienceDirect

Chinese Journal of Chemical Engineering

journal homepage: www.elsevier.com/locate/CJChE

Full Length Article

Facile purification and immobilization of organophosphorus hydrolase on protein-inorganic hybrid phosphate nanosheets

Zhenfu Wang [#], Jie Gao [#], Qinghong Shi, Xiaoyan Dong [*], Yan Sun

Department of Biochemical Engineering, School of Chemical Engineering and Technology and Key Laboratory of Systems Bioengineering and Frontiers Science Center for Synthetic Biology (Ministry of Education), Tianjin University, Tianjin 300350, China

ARTICLE INFO

Article history:
Received 14 December 2021
Received in revised form 17 July 2022
Accepted 17 July 2022
Available online 22 July 2022

Keywords:
Calcium phosphate nanocrystal (CaPs)
Biomimetic mineralization
Organophosphorus hydrolase (OPH)
Oriented immobilization
Hydrolysis
Methyl parathion

ABSTRACT

Oriented immobilization of enzymes helps to maintain their native structure and proper orientation for high-performance engineering to meet extensive biocatalysis demands. However, the supporting materials used for orientated immobilization are usually costly or complicated in preparation, affecting their practical applications. In this work, a facile purification and immobilization method was proposed for enzyme immobilization based on organic–inorganic hybrid calcium phosphate nanocrystal (CaPs) induced by Cu^{2+} modified bovine serum albumin (BSA-Cu). Then, the as-prepared hybrid calcium phosphate nanosheet, BSA-Cu@CaPs, was utilized for one-pot purification and immobilization of His-tagged organophosphorus hydrolase (OPH) by metal-affinity binding to the incorporated BSA. BSA-Cu@CaPs-OPH exhibited enhanced pH stability and thermal stability compared to the free enzyme. Moreover, BSA-Cu@CaPs-OPH could retain more than 75% and 56% of initial activity after reuse 5 and 10 times, respectively. The results demonstrated that this facile strategy was promising for the effective biodegradation of organophosphorus pesticides with the immobilized enzyme.

1. Introduction

Organophosphates (OPs) have been widely applied as pesticides in agriculture, however, the residual pesticides accumulated in the food chain exhibit a serious threat to the environment and human health [1]. Organophosphorus hydrolase (OPH) is a promising enzyme to detoxify OPs and has been extensively utilized to hydrolyze organophosphorus compounds due to its excellent efficiency and mild reaction conditions [2]. Nonetheless, poor stability and high cost of free enzyme restricted its large-scale applications. To date, multifarious methods have been developed for OPH immobilization such as physical adsorption or covalent coupling to the Supplementary Material and encapsulation in networks [3–6]. However, the random orientation of the immobilized enzyme molecules by these methods indicates that apparent enzyme activity might be inhibited due to the wrong combination (namely, the amino acid residues that act as the "active center" are involved in enzyme-carrier conjugation) [7] or improper orientations of enzyme molecules [8]. Besides, the initial enzyme solution used for immobilization usually is often purified in advance to reduce side reactions catalyzed by other enzymes, illuminating a time-consuming and expensive pre-purification process. Hence, a specific and efficient enzyme immobilization strategy that allows direct and orientated immobilization of the target enzymes from cell lysates is highly desired.

In recent years, affinity tags have emerged as an effective tool for recombinant protein purification [9]. Among them, the polyhistidine affinity tag, known as His-tag, is the most widely used because of its minimal effects on the transcription, translation and expression of the target protein, and strong affinity interaction with chelated transition metal ions (*e.g.*, Ni^{2+}, Cu^{2+}, and Co^{2+}) [10], which endows the immobilized metal-iron affinity chromatography with high binding specificity, mild purification conditions, and simple purification steps [11]. Hence, enzyme immobilization methods based on His-tag could allow simultaneous purification and orientated immobilization of the enzyme from cell lysates simultaneously, thus avoiding pre-purification and enzyme denaturation. Igor and coworkers fabricated a hybrid nanoparticle peptide-DNA scaffolded architectures by modifying a semiconductor quantum dot (QD) with peptide-DNA linkers for the immobilization of His-tagged phosphotriesterase [12]. Jiang and coworkers employed Ni-nitrilotriacetic acid-modified virus-like mesoporous silica nanoparticles [13], Fe-based metal–organic framework, MIL-88A [14], and yolk-shell Co/C@SiO_2@Ni/C

* Corresponding author. Fax: +86 22 27403389.
E-mail address: d_xy@tju.edu.cn (X. Dong).
# These authors contributed equally to this work.

https://doi.org/10.1016/j.cjche.2022.07.017
1004-9541/

nanoparticles [15] as the carriers for selective oriented immobilization of His-tagged organophosphohydrolase from *Agrobacterium radiobacter* P230. These studies strongly prove the efficiency of the oriented enzyme immobilization strategy based on His-tag. However, the aforementioned Supplementary Material are often costly or fabricated *via* complicated processes, which restrain their extensive applications in enzyme immobilization and the degradation of organophosphorus pesticides. Thus, it deserves to develop a versatile and green matrix material for purifying and immobilizing His-tagged OPH protein.

Calcium phosphate nanocrystal (CaPs), as the main inorganic component of animal bones, owns great biocompatibility and operational stability, simple preparation, and low price [16]. These characteristics make CaPs a promising matrix candidate in the development of enzyme immobilization. Recent studies have employed CaPs as the supporting matrix for enzymes, such as lipase [17], phytase [18], xylanase [19], and β-Glucosidase [20]. Herein, by *in situ* encapsulating bovine serum albumin (BSA) derivatives in CaPs *via* biomimetic mineralization, a CaPs-based organic–inorganic hybrid material, BSA-Cu@CaPs, was designed and fabricated for simultaneous purification and orientated immobilization of His-tagged OPH from the cell lysates due to the Cu^{2+} ion binding to the incorporated BSA. In addition, BSA-Ni@CaPs and BSA-induced copper phosphate nanocrystal (BSA@CuPs) were also synthesized for comparison. The great biocompatibility of CaPs allows the immobilized OPH on BSA-Ni@CaPs and BSA-Cu@CaPs to maintain activity. Finally, the immobilized His-tagged OPH was applied for the enzymatic degradation of methyl parathion (MP).

2. Material and Methods

2.1. Materials

BSA, iminodiacetic acid (IDA), 1,4-butanediol diglycidyl ether, Coomassie brilliant blue G-250, alcohol, phosphoric acid, NaOH, and hydroxyethyl piperazine ethanesulfonic acid (HEPES) were obtained from Sigma-Aldrich (New York, USA). $CaCl_2$, $CuCl_2$, $Cu(CH_3COO)_2$, $Ni(CH_3COO)_2{\cdot}H_2O$, iminazole, and 4-nitrophenol (4-NP) were purchased from Heowns (Tianjin, China). MP was received from Dr. Ehrenstorfer GmbH (Augsburg, Germany). Other chemicals were all of the highest purity available from local sources.

2.2. Synthesis of metal ion-modified BSA

BSA modified by IDA (BSA-IDA) was first synthesized as the previous report with some modifications [21]. BSA was modified by IDA with 1,4-butanediol diglycidyl ether as a linker to realize the reaction between the epoxy group and amine or imino group. In detail, 0.22 ml 1,4-butanediol diglycidyl ether was slowly added to the BSA solution at a concentration of 10 $mg{\cdot}ml^{-1}$ in 0.2 $mol{\cdot}L^{-1}$ borate buffer (pH 9.0). The reaction mixture was kept at 37 °C in a water bath. After 12 h reaction, the unreacted ether was removed by dialyzing with 0.2 $mol{\cdot}L^{-1}$ borate buffer (pH 9.0). Then, 0.4 g IDA was added to the intermediate product solution. After reaction at 37 °C for 24 h, the product solution was dialyzed using water to remove the uncombined IDA. Finally, excess $Cu(CH_3COO)_2$ or $Ni(CH_3COO)_2{\cdot}H_2O$ was added into the reaction system. After 1 h incubation at 25 °C, the product solution was dialyzed with water to remove the free Cu^{2+}. The obtained BSA derivatives were dried under vacuum for 48 h, which were marked as BSA-Cu and BSA-Ni, respectively. Zeta potentials of BSA and its derivatives were measured on a Zetasizer Nano Malvern Instruments (Worcestershire, U.K.).

2.3. Synthesis and characterization of CaPs and CuPs

The CaPs materials induced by BSA, BSA-Ni, and BSA-Cu (marked as BSA@CaPs, BSA-Ni@CaPs, and BSA-Cu@CaPs) were synthesized according to the literature with slight modifications [22]. In a typical procedure, 100 μl of $CaCl_2$ solution (200 $mmol{\cdot}L^{-1}$) was added into BSA, BSA-Ni, or BSA-Cu solution at a concentration of 0.1 $mg{\cdot}ml^{-1}$ in 10 $mmol{\cdot}L^{-1}$ PB (pH 7.4). After incubation at 4 °C for 48 h, the resulting precipitates were collected, washed, and dried under vacuum for 48 h. BSA@CuPs was synthesized by replacing $CaCl_2$ with $CuCl_2$ and induced by pristine BSA following the procedure described in literature [23]. Scanning electron microscopy (SEM) images and energy-dispersive X-ray (EDX) analysis of BSA-Ni@CaPs, BSA-Cu@CaPs, and BSA@CuPs were recorded on a Hitachi S4800 microscope (Tokyo, Japan). Transmission electron microscopy (TEM) micrographs of these samples were obtained with a Jeol JEM-2100 microscope (Tokyo, Japan). Their X-ray diffraction (XRD) patterns were recorded using a Bruker D&advance X-ray diffractometer (Billerica, USA). Fourier transform infrared spectroscopy (FT-IR) spectra were measured with a Perkin Elmer Spectrum 100 spectrometer (Wellesley, USA).

2.4. Purification and immobilization of OPH

Recombinant OPH with His-tag from *Pseudomonas diminuta* was expressed in *E. coli* Rosetta (DE3) harboring the plasmid pET-20b, and the crude OPH and pure OPH solutions were prepared as a previous report [24]. The fabrication of BSA-Cu@CaPs-OPH was presented in detail as representation only. BSA-Cu@CaPs (5 mg) was dispersed in 1 ml of 50 $mmol{\cdot}L^{-1}$ HEPES buffer (pH 8.5) and mixed with 1 ml of crude enzyme solution. The obtained mixture was incubated at 4 °C for 1 h. The precipitate was obtained by centrifugation and washed five times with 50 $mmol{\cdot}L^{-1}$ HEPES buffer (pH 8.5) containing 500 $mmol{\cdot}L^{-1}$ NaCl to remove the protein adsorbed on carriers by electrostatic adsorption and weak interactions. Finally, the precipitate was dried under vacuum for 24 h. The enzyme loading was determined by the Bradford assay method. The preparation of BSA@CaPs-OPH, BSA-Ni@CaPs-OPH, and BSA@CuPs-OPH was following the same methods. Then, immobilized OPH was washed with 50 $mmol{\cdot}L^{-1}$ HEPES buffer (pH 8.5) containing 500 $mmol{\cdot}L^{-1}$ imidazole to release the bounded OPH, and the collected enzyme solutions were analyzed by sodium dodecyl sulfate polyacrylamide gel electrophoresis (SDS-PAGE). Non-His-tagged OPH was expressed and the crude OPH was incubated with these hybrid carriers for OPH immobilization following the same procedure as in the preparation of BSA-Ni@CaPs-OPH and BSA@CuPs-OPH.

2.5. Activity assay and stabilities of free and immobilized OPH

The hydrolysis activities of free OPH, BSA@CaPs-OPH, BSA-Ni@CaPs-OPH, BSA-Cu@CaPs-OPH, and BSA@CuPs-OPH were investigated by the same methods. The activities measurement of BSA-Cu@CaPs-OPH was presented in detail as representation only. The activity of BSA-Cu@CaPs-OPH was assayed in 50 $mmol{\cdot}L^{-1}$ HEPES buffer (pH 8.5) containing 0.38 $mmol{\cdot}L^{-1}$ MP. After reacting for 1 min, trichloroacetic acid solution (10% (mass)) was utilized to terminate the enzymatic reaction. The mixture was separated by centrifugation (10000 g, 1 min) and the absorbance of the supernatant containing 4-NP was measured at 410 nm by a spectrophotometric method. One unit of OPH activity was defined as the enzyme mass that produced 1 μmol of 4-NP per minute. The Michaelis-Menten kinetic parameters were determined by measuring the activities of free and immobilized OPH using MP as substrate (0.038–0.38 $mmol{\cdot}L^{-1}$). The enzymatic hydrolysis could be expressed by the Michaelis-Menten equation Eq. (1),

$$v = V_{max}[S]/(K_m + [S]) \quad (1)$$

where v denotes the initial hydrolysis rate, V_{max} is the maximum hydrolysis velocity, K_m is the Michaelis-Menten constant, $[S]$ represents MP concentration. Besides, k_{cat} was calculated by using Eq. (2).

$$k_{cat} = V_{max}/[E] \quad (2)$$

where $[E]$ represents OPH concentration.

The thermal stability of the free OPH and immobilized OPH was investigated by incubating them for 1 h in 50 mmol·L^{-1} HEPES buffer (pH 8.5) at 25–70 °C. Their pH tolerance was determined by immersing the samples for 1 h in 50 mmol·L^{-1} PB buffer (pH 6–8) or 50 mmol·L^{-1} glycine-NaOH buffer (pH 9–10.5) at 25 °C, respectively. To investigate the repeatability of immobilized OPH, after measuring the initial activity assay, the reaction mixture was centrifuged and the obtained precipitation was washed three times. After centrifugation, the obtained catalyst was used in the next degradation cycle under the same conditions.

3. Results and Discussion

3.1. Characterization of carriers and immobilized OPH

The modification methods of BSA with Ni^{2+} and Cu^{2+} were shown in Fig. 1. Zeta potential values of BSA and its derivatives

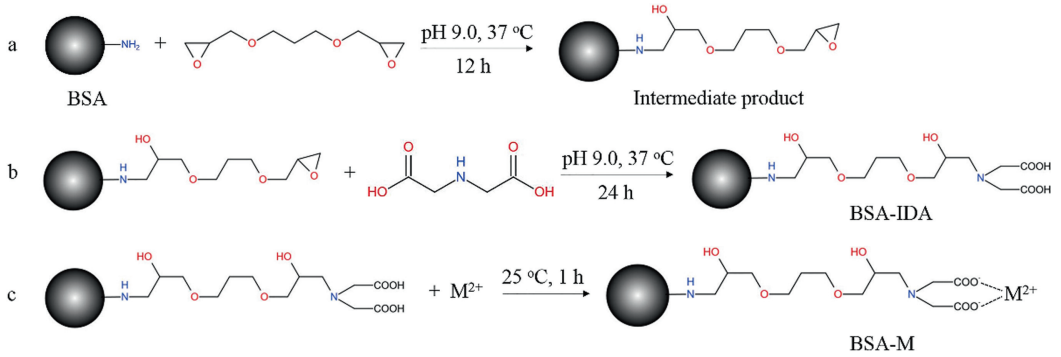

Fig. 1. Synthetic routes for the modification of BSA with IDA and metal ions (M^{2+} = Ni^{2+} or Cu^{2+}).

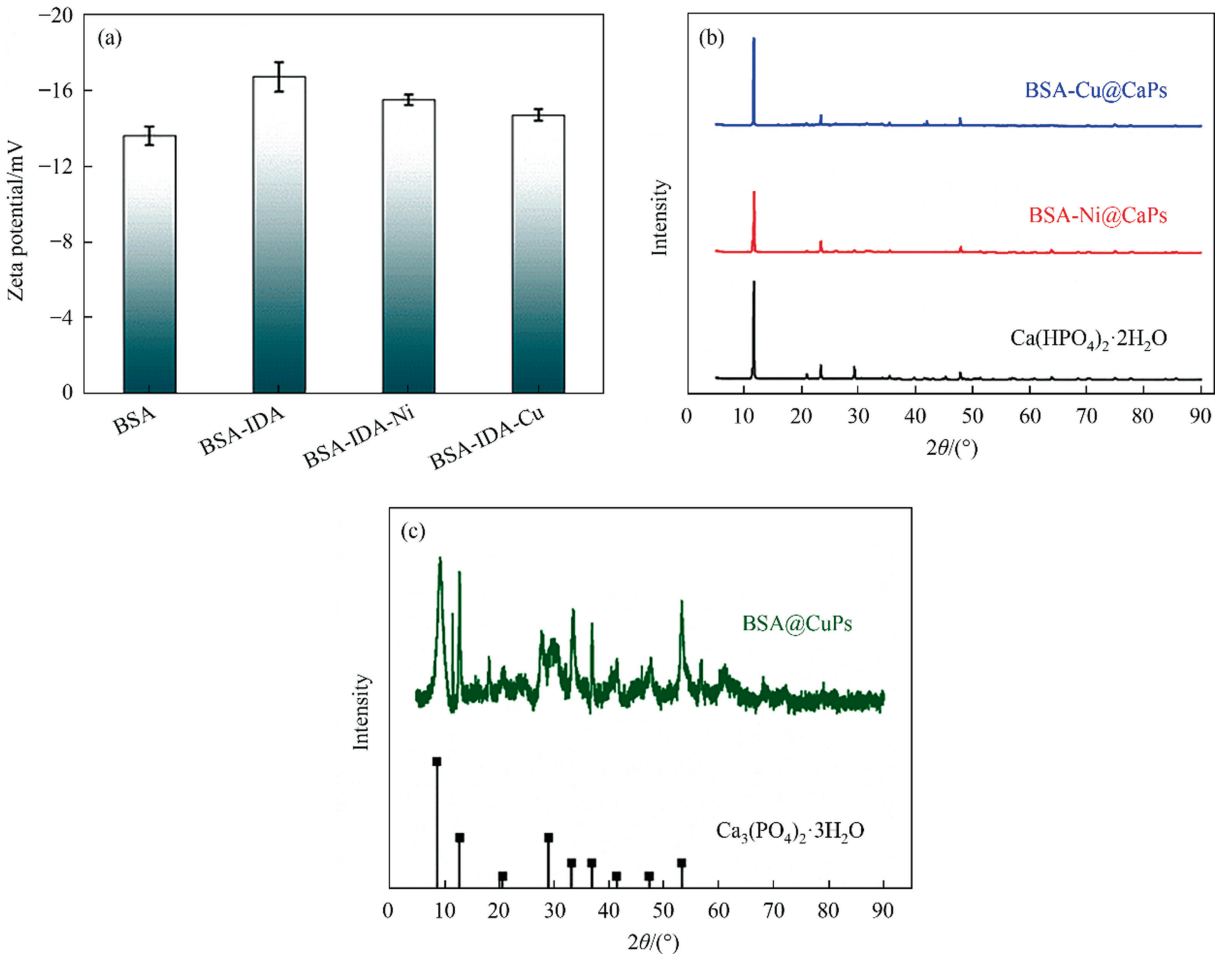

Fig. 2. (a) Zeta potentials of BSA and their derivatives. XRD patterns of (b) BSA-Ni@CaPs, BSA-Cu@CaPs, and (c) BSA@CuPs.

were measured, as depicted in Fig. 2(a). The native BSA exhibited negative charges due to its isoelectric point of 4.7, while BSA-IDA displayed a lower zeta potential than that of pristine BSA after IDA modification. The decrease was due to the presence of two carboxyl groups in IDA that was modified on the BSA surface, suggesting successful chemical modifications of the protein. After incubation with Ni^{2+} and Cu^{2+}, the resulted proteins showed slightly decreased zeta potential (Fig. 2(a)), resulting from effective binding between BSA-IDA and metal ions.

Then, hybrid organic–inorganic nanosheets were prepared using pristine or modified BSA as the organic components and CaPs or CuPs as the inorganic components. As illustrated in Fig. S1 (Supplementary Material), SEM images of BSA-Ni@CaPs, BSA-Cu@CaPs, and BSA@CuPs show the morphology of nanosheets. As shown in Fig. 2(b) and 2(c), XRD patterns of these nanocomposites matched well with the crystal pattern from $Ca(HPO_4)_2{\cdot}2H_2O$ (JCPDS 72-0713) [25] or $Cu_3(PO_4)_2{\cdot}3H_2O$ (JCPDS 00-022-0548) [26]. Moreover, the sharp and strong peaks of these samples (Fig. 2(b) and 2(c)) indicated that the hybrid nanosheets were well crystallized after the incorporation of BSA or its derivatives. The elemental compositions of BSA-Ni@CaPs, BSA-Cu@CaPs, and BSA@CuPs were exhibited in Fig. S2. The results of elemental mapping validated the presence of $Ca(HPO_4)_2{\cdot}2H_2O$ or $Cu_3(PO_4)_2{\cdot}3H_2O$ components in the corresponding hybrid materials. As depicted in Fig. S3(a), BSA-Ni@CaPs, BSA-Cu@CaPs, and BSA@CuPs were identified to show type-IV N_2 adsorption isotherms with obvious hysteresis loops, suggesting the existence of mesoporous structures [27]. Their BET surface area increased in the order of BSA-Ni@CaPs < BSA-Cu@CaPs < BSA@CuPs (Fig. S3(b)), while Fig. S3(c) further confirms the mesoporous structures (pore diameter >2 nm) in these samples.

The FT-IR spectroscopy provided direct proofs for the preparation of the hybrid organic–inorganic nanosheets and OPH immobilization on the hybrid materials. As shown in Fig. 3. The P—O vibrations and stretches were observed at 559 and 630 cm^{-1}, 995 and 1030 cm^{-1}, respectively, indicating the existence of phosphate groups. The vibration bands at 1534 cm^{-1} and 1652 cm^{-1} were attributed to the amide I and amide II bands of the incorporated BSA or modified BSA, which proved that BSA molecules were incorporated by the self-assembly of protein and inorganic ligand (Fig. 3). The obviously enhanced peaks around 1534 cm^{-1} suggested successful OPH immobilization on these hybrid carriers (Fig. 3(a)–(c)).

To verify the selectivity of the immobilization process, excess iminazole solution (500 $mmol{\cdot}L^{-1}$) was utilized to elute the adsorbed OPH by affinity interaction. SDS-PAGE analysis (Fig. 4) showed that His-tagged OPH could be directly and selectively separated from the crude enzyme solution and immobilized on BSA-

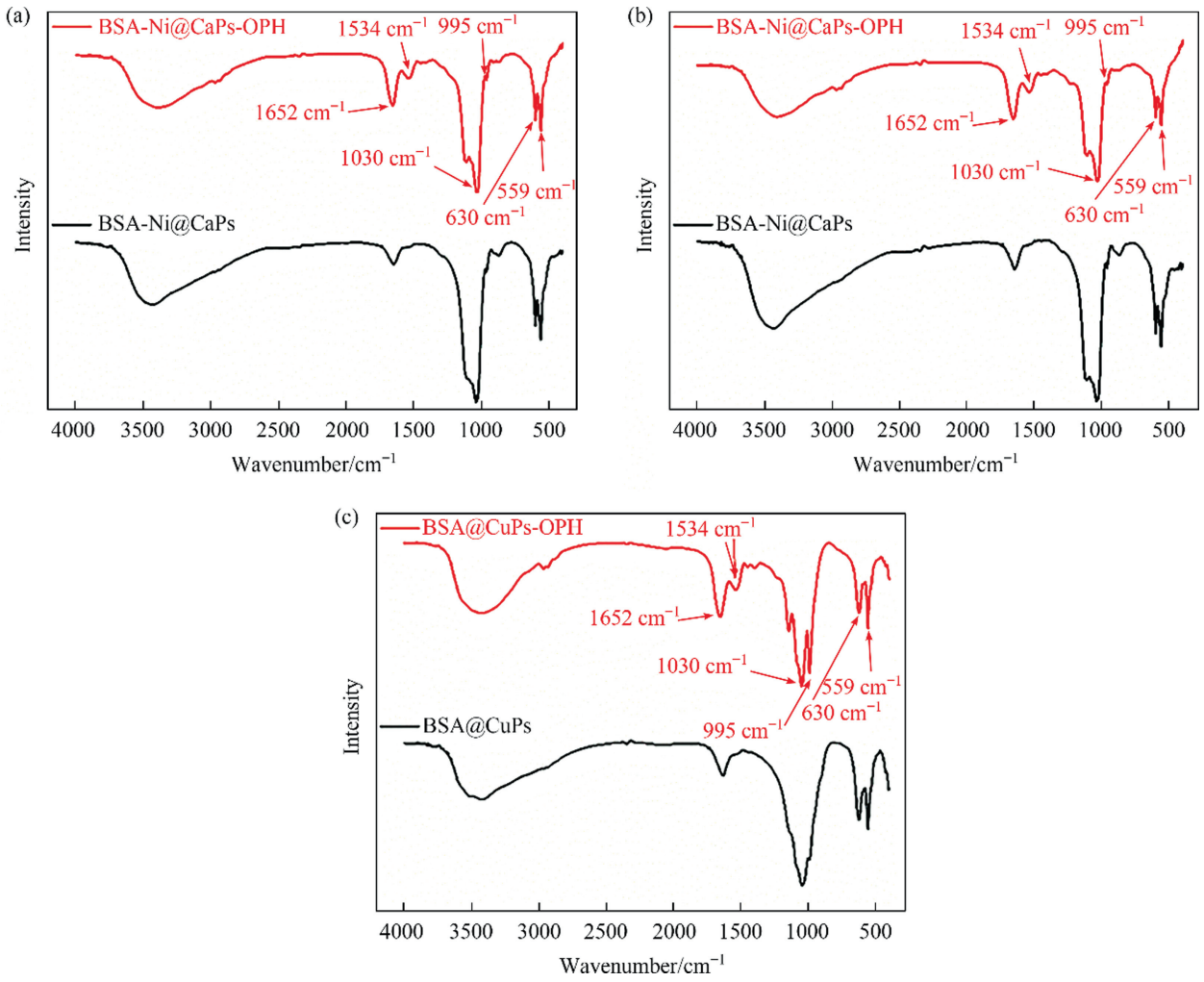

Fig. 3. FT-IR spectra of (a) BSA-Ni@CaPs and BSA-Ni@CaPs-OPH, (b) BSA-Cu@CaPs and BSA-Cu@CaPs-OPH, (c) BSA@CuPs and BSA@CuPs-OPH.

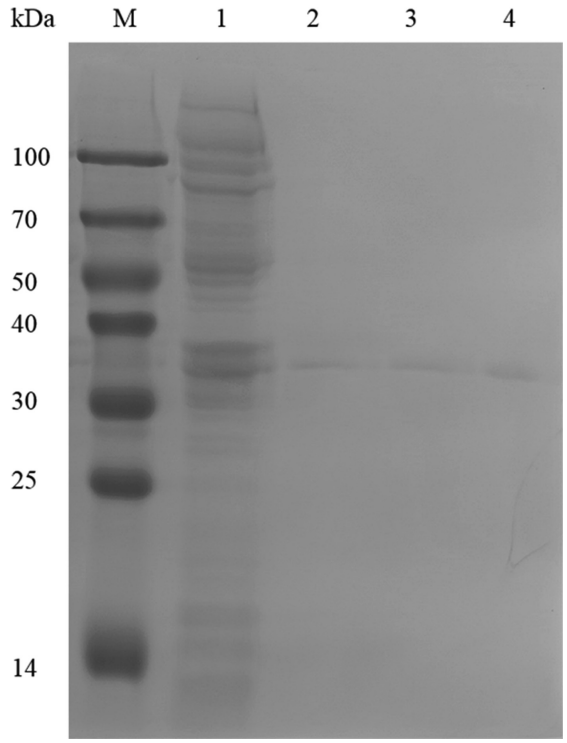

Fig. 4. SDS-PAGE analysis. Lane M, marker; lane 1, crude cell lysate; lane 2, eluted protein from BSA-Ni@CaPs-OPH; lane 3, eluted protein from BSA-Cu@CaPs-OPH; lane 4, eluted protein from BSA@CuPs-OPH. Elution was done with 500 mmol·L^{-1} imidazole in 50 mmol·L^{-1} HEPES buffer (pH 8.5).

Ni@CaPs, BSA-Cu@CaPs, and BSA@CuPs due to the high affinity of histidine toward Ni^{2+} or Cu^{2+}. Moreover, the contribution of electrostatic adsorption on enzyme immobilization was minimized by washing the obtained BSA-Ni@CaPs-OPH, BSA-Cu@CaPs-OPH, and BSA@CuPs-OPH with 50 mmol·L^{-1} HEPES buffer (pH 8.5) containing 500 mmol·L^{-1} NaCl. The obtained BSA@CaPs-OPH did not exhibit loading of His-tagged OPH (data not shown), demonstrating that no His-tagged OPH was bounded on BSA@CaPs. Non-His-tagged OPH was also expressed and the crude OPH was incubated with these hybrid carriers. However, no OPH was successfully immobilized on BSA-Ni@CaPs, BSA-Cu@CaPs, and BSA@CuPs (data not shown). Therefore, BSA-Ni@CaPs, BSA-Cu@CaPs, and BSA@CuPs could be utilized for one-step purification and immobilization of His-tagged proteins as expected.

3.2. Catalysis performances of the free and immobilized OPH

Table S1 shows the enzyme loading and relative activities of immobilized OPH with different carriers. The OPH loading of BSA@CuPs-OPH was higher than BSA-Ni@CaPs-OPH and BSA-Cu@CaPs-OPH, which might be attributed to the higher metal content on the carrier's surface (Fig. S2) and higher BET surface area than BSA-Ni@CaPs and BSA-Cu@CaPs (Fig. S3(b)), suggesting more immobilization sites for His-tagged OPH. Nevertheless, the reactive activity of BSA@CuPs-OPH was much lower than those of BSA-Ni@CaPs-OPH and BSA-Cu@CaPs-OPH.

Kinetic parameters of free and immobilized OPH with MP were investigated. As depicted in Table 1, the K_m values of BSA-Ni@CaPs-OPH and BSA-Cu@CaPs-OPH were lower than that of free OPH, while the K_m value of BSA@CuPs-OPH was higher than that of free OPH. It indicated that BSA-Ni@CaPs-OPH and BSA-Cu@CaPs-OPH owned higher substrate affinity compared to free OPH and BSA@CuPs-OPH. However, all the immobilized OPH showed lower k_{cat} and k_{cat}/K_m than free OPH. The reason might be that negative conformation changes occurred in OPH protein after immobilization on the carriers, thus decreasing the enzyme activity.

The thermal stability of free and immobilized OPH was then evaluated. As depicted in Fig. 5(a), the residual enzymatic activity decreased with the increasing incubation temperature for both the free and immobilized OPH, while BSA-Cu@CaPs-OPH showed better thermal stability than other catalysts. Notably, the residual activity of free OPH, BSA-Ni@CaPs-OPH, and BSA@CuPs-OPH decreased below 20%, 30%, and 5% at 60 °C, respectively, while BSA-Cu@CaPs-OPH exhibited higher residual activity (over 60%) than the above samples (Fig. 5(a)). It suggests that BSA-Cu@CaPs was able to stabilize the enzyme and relieve the activity decline at high temperatures.

The solution pH could significantly affect the enzyme activity by altering the dissociation of the necessary groups of the active center. As shown in Fig. 5(b), the relative activity of free OPH after acid incubation was lower than that of the sample after alkaline incubation, illustrating that OPH exhibited better tolerance to the alkaline than the acid environment. Compared with free OPH, the alkaline tolerance of the immobilized OPH was enhanced with the aid of CaPs or CuPs (Fig. 5(b)), which might be attributed to the abundant hydroxyl groups on the phosphate crystals, thus resulting in a change in the microenvironment of the enzyme molecule. It should also be mentioned that BSA-Cu@CaPs-OPH showed improved both acid and alkaline tolerance (Fig. 5(b)), which demonstrated the stabilization effect of BSA-Cu@CaPs on the conformation of the enzyme protein.

The reusability of immobilized enzyme is critical for their industrial applications. As presented in Fig. 5(c), the residual activities of BSA-Ni@CaPs-OPH, BSA-Cu@CaPs-OPH, and BSA@CuPs-OPH after repeat uses were measured. After being reused 5 times, BSA-Ni@CaPs-OPH and BSA-Cu@CaPs-OPH maintained more than 60% of their original activity after five cycles, while the residual activity of BSA@CuPs-OPH decreased to ~20% (Fig. 5(c)). After repeated use 10 times, the residual activity of BSA-Cu@CaPs-OPH enzyme activity was still 56.77% (Fig. 5(c)). The above results proved that BSA-Cu@CaPs was conducive to improving the stability of the immobilized OPH against extreme conditions and BSA-Cu@CaPs-OPH would be a good nanobiocatalyst for the biodegradation of organophosphorus pesticides.

Table 1
Kinetic parameters for free and immobilized OPH

	V_{max}/mmol·L^{-1}·s^{-1}	K_m/mmol·L^{-1}	k_{cat}/min^{-1}	(k_{cat}/K_m)/L·min^{-1}·mmol^{-1}
OPH	16.91	0.54	6362	11822
BSA-Ni@CaPs-OPH	50.23	0.33	2700	8171
BSA-Cu@CaPs-OPH	36.08	0.35	1767	5004
BSA@CuPs-OPH	17.62	1.38	525	380

Note: Reaction conditions is 0.25 μmol·L^{-1} OPH in 50 mmol·L^{-1} HEPES buffer (pH 8.5), 25 °C.

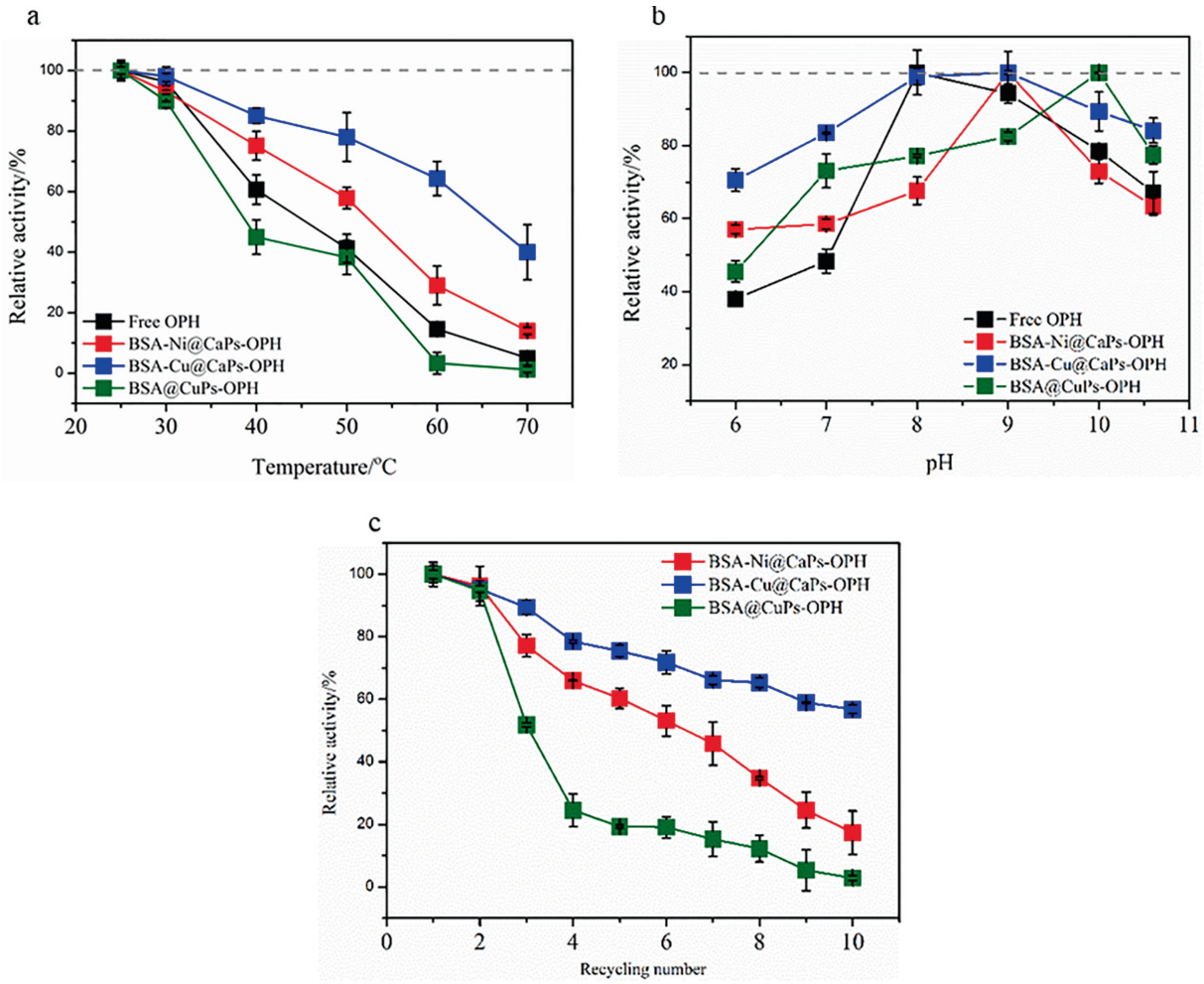

Fig. 5. Stabilities of the free and immobilized OPH, (a) thermal stability, (b) pH tolerance, and (c) reusability. Reaction conditions: 0.25 μmol·L^{-1} OPH, 0.38 mmol·L^{-1} MP, 25 °C. Error bars represent standard deviations from triplicate experiments.

4. Conclusions

In summary, BSA-Ni@CaPs, BSA-Cu@CaPs, and BSA@CuPs were synthesized via biomimetic mineralization method and employed for the direct and orientated immobilization of His-tagged OPH from cell lysates without any pre-purification based on the affinity between the His-tagged OPH and Ni^{2+} or Cu^{2+} on the surface of hybrid phosphate nanocrystals. Among these immobilized enzymes, BSA-Ni@CaPs-OPH and BSA-Cu@CaPs-OPH owned lower K_m values and higher affinity to the substrate than free OPH. BSA-Cu@CaPs-OPH exhibited improved thermal and pH stability. Moreover, BSA-Cu@CaPs-OPH displayed higher stability in repeat uses than BSA-Ni@CaPs-OPH and BSA@CuPs-OPH. These results suggested that the hybrid CaPs nanocrystal, especially BSA-Cu@CaPs, could be good candidates for facile purification and immobilization of His-tagged enzymes with high activity and stability in extensive applications.

Data Availability

Data will be made available on request.

Declaration of Competing Interest

The authors declare that they have no known competing financial interests or personal relationships that could have appeared to influence the work reported in this paper.

Acknowledgements

This work was supported by the National Key Research and Development Program of China (2021YFC2102801) and the National Natural Science Foundation of China (21621004).

Supplementary Material

Supplementary data to this article can be found online at https://doi.org/10.1016/j.cjche.2022.07.017.

References

[1] K. Kim, O.G. Tsay, D.A. Atwood, D.G. Churchill, Destruction and detection of chemical warfare agents, *Chem. Rev.* 111 (9) (2011) 5345–5403.
[2] L.J. Wang, Y. Sun, Engineering organophosphate hydrolase for enhanced biocatalytic performance: a review, *Biochem. Eng. J.* 168 (2021) 107945.
[3] K. El-Boubbou, D.A. Schofield, C.C. Landry, Enhanced enzymatic activity of OPH in ammonium-functionalized mesoporous silica: surface modification and pore effects, *J. Phys. Chem. C* 116 (33) (2012) 17501–17506.
[4] L. Han, A.H. Liu, Novel cell-inorganic hybrid catalytic interfaces with enhanced enzymatic activity and stability for sensitive biosensing of paraoxon, *ACS Appl. Mater. Interfaces* 9 (8) (2017) 6894–6901.
[5] H. Cheng, Y.L. Zhao, X.J. Luo, D.S. Xu, X. Cao, J.H. Xu, Q. Dai, X.Y. Zhang, J. Ge, Y.P. Bai, Cross-linked enzyme-polymer conjugates with excellent stability and detergent-enhanced activity for efficient organophosphate degradation, *Bioresour. Bioprocess.* 5 (2018) 49.
[6] M. Sharifi, S.M. Robatjazi, M. Sadri, J.M. Mosaabadi, Immobilization of organophosphorus hydrolase enzyme by covalent attachment on modified cellulose microfibers using different chemical activation strategies:

Characterization and stability studies, *Chin. J. Chem. Eng.* 27 (1) (2019) 191–199.
[7] D.F. Kienle, R.M. Falatach, J.L. Kaar, D.K. Schwartz, Correlating structural and functional heterogeneity of immobilized enzymes, *ACS Nano* 12 (8) (2018) 8091–8103.
[8] E. Steen Redeker, D.T. Ta, D. Cortens, B. Billen, W. Guedens, P. Adriaensens, Protein engineering for directed immobilization, *Bioconjug. Chem.* 24 (11) (2013) 1761–1777.
[9] S. Mahmoodi, M. Pourhassan-Moghaddam, D.W. Wood, H. Majdi, N. Zarghami, Current affinity approaches for purification of recombinant proteins, *Cogent Biol.* 5 (1) (2019) 1665406.
[10] X.Y. Zhao, G.S. Li, S.F. Liang, Several affinity tags commonly used in chromatographic purification, *J. Anal. Methods Chem.* 2013 (2013) 581093.
[11] H. López-Laguna, E. Voltà-Durán, E. Parladé, A. Villaverde, E. Vázquez, U. Unzueta, Insights on the emerging biotechnology of histidine-rich peptides, *Biotechnol. Adv.* 54 (2022) 107817.
[12] J.C. Breger, S. Buckhout-White, S.A. Walper, E. Oh, K. Susumu, M.G. Ancona, I.L. Medintz, Assembling high activity phosphotriesterase composites using hybrid nanoparticle peptide-DNA scaffolded architectures, *Nano Futur.* 1 (1) (2017) 011002.
[13] L.Y. Zhou, J.J. Li, J. Gao, H. Liu, S.G. Xue, L. Ma, G.X. Cao, Z.H. Huang, Y.J. Jiang, Facile oriented immobilization and purification of his-tagged organophosphohydrolase on viruslike mesoporous silica nanoparticles for organophosphate bioremediation, *ACS Sustainable Chem. Eng.* 6 (10) (2018) 13588–13598.
[14] S.G. Xue, J.J. Li, L.Y. Zhou, J. Gao, G.H. Liu, L. Ma, Y. He, Y.J. Jiang, Simple purification and immobilization of his-tagged organophosphohydrolase from cell culture supernatant by metal organic frameworks for degradation of organophosphorus pesticides, *J. Agric. Food Chem.* 67 (49) (2019) 13518–13525.
[15] Y.X. Li, P.Q. Luan, L.Y. Zhou, S.G. Xue, Y.H. Liu, Y.T. Liu, Y.J. Jiang, J. Gao, Purification and immobilization of His-tagged organophosphohydrolase on yolk–shell Co/C@SiO_2@Ni/C nanoparticles for cascade degradation and detection of organophosphates, *Biochem. Eng. J.* 167 (2021) 107895.
[16] C. Qi, J. Lin, L.H. Fu, P. Huang, Calcium-based biomaterials for diagnosis, treatment, and theranostics, *Chem. Soc. Rev.* 47 (2) (2018) 357–403.
[17] J. Trbojević Ivić, D. Veličković, A. Dimitrijević, D. Bezbradica, V. Dragačević, M. Gavrović Jankulović, N. Milosavić, Design of biocompatible immobilized *Candida rugosa* lipase with potential application in food industry, *J. Sci. Food Agric.* 96 (12) (2016) 4281–4287.
[18] T.C. Coutinho, P.W. Tardioli, C.S. Farinas, Phytase immobilization on hydroxyapatite nanoparticles improves its properties for use in animal feed, *Appl. Biochem. Biotechnol.* 190 (1) (2020) 270–292.
[19] T.C. Coutinho, P.W. Tardioli, C.S. Farinas, Hydroxyapatite nanoparticles modified with metal ions for xylanase immobilization, *Int. J. Biol. Macromol.* 150 (2020) 344–353.
[20] T.C. Coutinho, M.J. Rojas, P.W. Tardioli, E.C. Paris, C.S. Farinas, Nanoimmobilization of β-glucosidase onto hydroxyapatite, *Int. J. Biol. Macromol.* 119 (2018) 1042–1051.
[21] B.L. Xie, H. Zhang, X. Li, X.Y. Dong, Y. Sun, Iminodiacetic acid-modified human serum albumin: a multifunctional agent against metal-associated amyloid β-protein aggregation and cytotoxicity, *ACS Chem. Neurosci.* 8 (10) (2017) 2214–2224.
[22] A.H. Memon, R.S. Ding, Q.P. Yuan, Y. Wei, H. Liang, Facile synthesis of alcalase-inorganic hybrid nanoflowers used for soy protein isolate hydrolysis to improve its functional properties, *Food Chem.* 289 (2019) 568–574.
[23] J. Ge, J.D. Lei, R.N. Zare, Protein–inorganic hybrid nanoflowers, *Nat. Nanotechnol.* 7 (7) (2012) 428–432.
[24] G.A. Omburo, J.M. Kuo, L.S. Mullins, F.M. Raushel, Characterization of the zinc binding site of bacterial phosphotriesterase, *J. Biol. Chem.* 267 (19) (1992) 13278–13283.
[25] L.B. Wang, Y.C. Wang, R. He, A.W. Zhuang, X.P. Wang, J. Zeng, J.G. Hou, A new nanobiocatalytic system based on allosteric effect with dramatically enhanced enzymatic performance, *J. Am. Chem. Soc.* 135 (4) (2013) 1272–1275.
[26] X.Z. Sun, H.Q. Niu, J.R. Song, D.H. Jiang, J. Leng, W. Zhuang, Y. Chen, D. Liu, H.J. Ying, Preparation of a copper polyphosphate kinase hybrid nanoflower and its application in ADP regeneration from AMP, *ACS Omega* 5 (17) (2020) 9991–9998.
[27] T.T. Wang, Z.K. Kou, S.C. Mu, J.P. Liu, D.P. He, I.S. Amiinu, W. Meng, K. Zhou, Z.X. Luo, S. Chaemchuen, F. Verpoort, 2D dual-metal zeolitic-imidazolate-framework-(ZIF)-derived bifunctional air electrodes with ultrahigh electrochemical properties for rechargeable zinc-air batteries, *Adv. Funct. Mater.* 28 (5) (2018) 1705048.